Battery Slurry Mixing Modelling

Internship Report

SIEMENS

RWTH AACHEN UNIVERSITY

Rishi Dhar

April 2023

Declaration by Manager

I hereby declare that Mr. Dhar has independently written the submitted report -including all enclosed materials - and has not used any sources or aids other than those listed in the bibliography. This work has not been submitted in the same or a similar form before. As Mr. Dhar's manager, after carefully examining the report, I grant him the permission to submit this work at the university

Signature: _____ Date: _____

Pasch Theresa Siemens, München

Declaration by Author

I declare that this work has been composed by me, and describes my own work, unless otherwise acknowledged in the text. All sentences or passages quoted in this paper from other people's work have been specifically acknowledged by clear cross-referencing to author, work and page(s). Any photos and illustrations which are not the work of the author have been used with the explicit permission of the originator and are specifically acknowledged. This work has not been and will not be submitted for any other degree or the obtaining of ECTS points at the RWTH Aachen University or any other institution of higher education.

Signature: _____ Date: _____

Rishi Dhar Siemens, München

Contents

List of Figures

Chapter 1

Introduction

The rise in the usage of appliances which run on stored electricity has led to an increased demand for energy storage solutions that are both efficient and dependable. Among the various options available, lithium-ion batteries have emerged as the clear front runner, thanks to their comparably high energy density, extended cycle life, and minimal self-discharge rate. These batteries have become ubiquitous in our daily lives, powering everything from smartphones and laptops to electric cars and renewable energy systems.[21]
Within the electric mobility space, lithium-ion batteries play an increasingly important role. They are utilized in electric bicycles, electric scooters. The automotive industry employs lithium-ion batteries within different kinds of hybrid vehicles as well as in plug-in hybrid vehicles and electric vehicles. In stationary applications, lithium-ion batteries are available as mini storage devices with around 2 kWh up to 40 MWh in larger plants. [21]
Nominal capacity, electric energy and power are the typical parameters used to characterize a battery cell or system. The amount of electric charge, a power source can deliver under specific discharge conditions describes its capacity . It depends on the discharging current, the cut-off voltage, the temperature, and the type and amount of active materials. The energy of a battery can be calculated as the product of average discharge voltage and capacity. Specific energy refers to the mass of the rechargeable battery. Energy density refers to the volume of the rechargeable battery. Power is calculated as the product of current and voltage, for instance, while discharging the product of the discharge current and voltage provides the power output. [13]
Any anomalies among the output parameters like specific energy can be directly linked to issues within the production process. Thus, an optimal production processes is necessary to avoid losses within the resulting cell capacity. Previous works have shown that the electrode structure is directly influenced by formulation parameters, such as the recipe of the slurry or process parameters of calendaring [2]. The structure of an electrode directly influences its resulting electrical, mechanical, and electro-chemical properties. Hence, in order to improve the structure, processes directly affecting the electrode production needs to be studied carefully.
The next section provides a brief introduction to the complete production chain which starts with slurry mixing. A typical battery slurry contains active materials, conductive additives and binders. Several research projects have already investigated the influence of the different active material type or additives [3] on electrode properties and cell performances. Some previous studies have shown that it is difficult to define a direct correlation between the process and the product because tracking every reaction between compounds to its element level is unfeasible. For example, graphite based anodes contain carboxymethyl cellulose (CMC) and styrene-butadiene rubber (SBR) as preferred binders, which allow for the elimination of N-Methyl-2-pyrrolidone (NMP) from the process but in the hindsight CMC results in poor usage of electro-active ma-

terials and poor rate capability of Si anodes [7]. Simulating the particle interactions for the active materials, binders and conductive materials can be done using Discrete Element Method (DEM) while the wetting agents which provide slurry with the viscosity can be modelled using Computational Fluid Dynamics(CFD). Coupling them [16] provides accurate insights about the fluid structure interaction and the inter dependencies. Numerous studies [5] state that when the volume percentage of solid and fluid are comparable and the particle size is comparable to 10^{-3}, considering a two-way coupling for calculating the turbulence created by particle fluid interaction becomes significant. Considering the particle size being in the range of 10μm, looking at slurries homogeneously becomes feasible. This also can be beneficial on multiple fronts, firstly, it is easier to monitor the behaviour of the slurry and secondly, it saves huge computational resources as the particles need not be computed as Lagrangian in nature.
Mixing of homogeneous fluids is a fundamental process in fluid dynamics that involves combining two or more fluids to achieve a uniform distribution of their constituents. It plays a crucial role in various scientific, industrial, and environmental applications. The process of mixing homogeneous fluids can occur through different mechanisms, depending on the specific conditions and characteristics of the fluids involved. One common mechanism is diffusion, where molecular motion leads to the random spreading of molecules from regions of high concentration to regions of low concentration. Diffusion alone being slow, is insufficient for achieving complete mixing. To enhance it, additional mechanisms such as convection and turbulence can be employed. While convection leads to the transport of fluid parcels, Turbulence refers to the chaotic and irregular fluid motion characterized by eddies and vortices. Turbulent flows are highly effective in promoting mixing as they enhance the intermingling of fluid particles. Some external parameters like mixers, agitators, or stirrers in industrial settings can also enhance mixing by imparting additional kinetic energy to the fluids, facilitating the break-up of larger fluid structures, and promoting inter-molecular collisions. In the case of battery, binders may be introduced to vary the mixing efficiency. These additives can alter the surface tension and inter-molecular forces within the fluid, reducing the resistance to mixing and promoting better homogenization. The characterization and analysis of mixing processes often involve the study of concentration gradients, flow patterns, and residence time distribution. Various factors influence the efficiency of mixing homogeneous fluids. The velocity and direction of fluid flow, the geometry of the mixing vessel or apparatus, and the properties of the fluids, such as viscosity and density, all play significant roles.

1.1 Battery Cell Production Process

A general battery production process involves two major steps, the cell production and cell assembly [1]. The cell production varies based on anode or cathode production, while the cell assembly refers to the arrangement and packing of the produced cells for optimized performance.

1.1.1 Cell Production Process

Electrode Material Preparation

The first step is to prepare the active electrode materials. For the cathode, commonly used materials are lithium cobalt oxide (LiCoO2), lithium nickel manganese cobalt oxide (NMC), or lithium iron phosphate (LiFePO4) [13]. For the anode, graphite is typically used. The active materials are processed to achieve the desired particle size, morphology, and composition.

Mixing

In this step, the active materials are mixed with binders, conductive additives, and solvents to create a slurry [6]. The binders, such as polyvinylidene fluoride (PVDF), help hold the active materials together, while the conductive additives, such as carbon black or carbon nanotubes, enhance the electrical conductivity of the electrode. The solvent helps create a uniform suspension of the components.

Coating

The slurry is then coated onto a substrate, like aluminium or copper [8]. The coating process can be performed using various techniques, such as doctor blade coating, slot die coating, or roll-to-roll coating. The slurry is uniformly spread onto the substrate, and excess solvent is removed through drying or solvent evaporation, leaving a solid electrode coating.

Drying

The drying process is a critical step in battery production, specifically in the manufacturing of electrode materials[14]. After the battery slurry is coated onto the current collector, the drying process is employed to remove the solvent and any volatile components from the slurry, leaving behind a solid and uniform electrode layer.

Calendering

To improve the electrode's density, mechanical strength, and electrical conductivity, the coated electrode may undergo a calendering process. Calendering involves passing the electrode through a set of rollers under pressure [14]. This process helps compress the electrode and enhances its overall performance.

Slitting

The electrodes up to this point will be in standard widths up to 1.5m. This stage runs along the length of the electrodes and cuts them down in width to match one of the final dimensions required for the cell.

1.1.2 Cell Assembly Process

Winding

Winding process involves the two electrode to move across separator webs around winding mandrel (prismatic cell) or center pin (cylindrical cell) with appropriate tension forces. [20].

Stacking

When the anode sheets and the cathode sheets are stretched with minimum surface damage ,they are moved alternating from left and right onto a z-folded separator. A cell stack can consist of up to 120 individual layers.

Packaging and Drying

The electrodes are then wound or stacked together to create a jellyroll or pouch configuration. Welding the electrodes with the cover and case needs to be precise as any air seepage can deteriorate the life cycle of the battery. The packaged batteries kept in vaccuum drying ovens to remove any humidity or moisture left before electrolyte can be filled.

Electrolyte Filling

Electorlyte solution is poured in the cell assembly with precise dosing in extremely dry atmosphere to avoid any air seepage.

Formation and aging

Allowing settling time for the electrolyte to fill all pores is essential. Hence the wetting time for a few days are provided to allow the electrolyte to settle in pores wihtin the battery enclosure.

Testing and grading

Tests such as pulse tests, internal resistance measurements (DC), optical inspections, OCV tests and leak tests are performed to assess the battery cell quality.

Lithium-ion battery cell production process

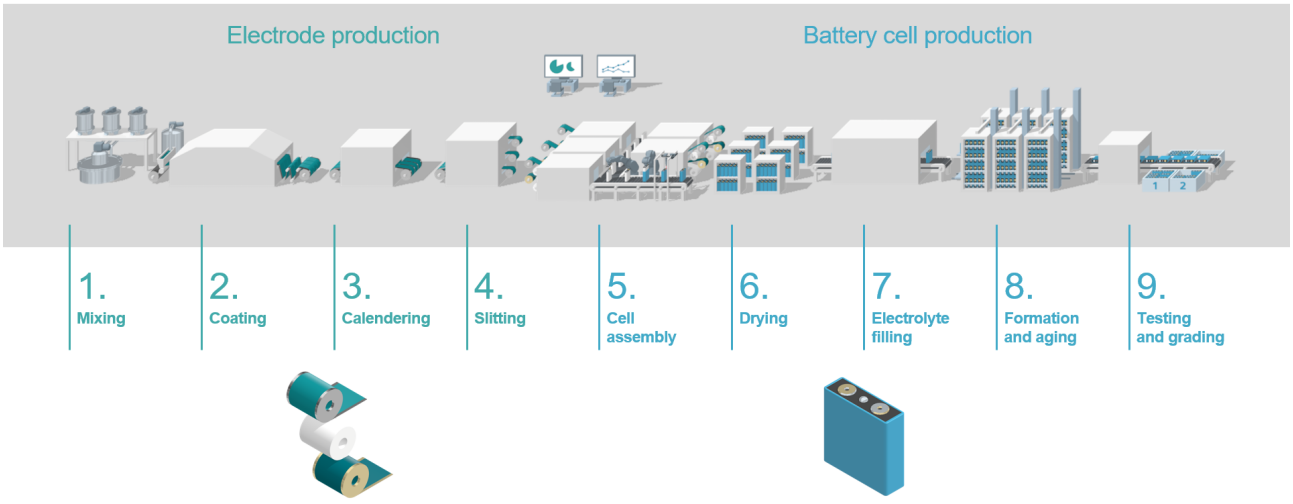

The next chapter describes the problem statement. Chapter 3 includes approaches towards fluid modelling and setting up the model. The chapter 4 describes task wise details with conclusion in chapter 5.

Chapter 2

Motivation

2.1 Influence of slurry on coating

In state-of-the-art production lines, lithium-ion battery electrode slurries are coated on a metallic substrate from a slot die, which is embedded in a large-scale roll-to-roll process chain [11]. Depending on the process parameters, different mechanisms cause the formation of defects. Parameters such as excessive flow rates or insufficient coating speeds may lead to varying coating direction. Another important parameter is a uniform slurry supply. To ensure a uniform coating layer, the slurry must be free of contaminants and show a homogeneous distribution of all components. Several pre-treatment steps must be performed, namely filtration in terms of solid containment and agglomerates, degassing in order to eliminate bubbles, and thermal control, as the viscosity strongly depends on the slurry's temperature. One of the most important process parameters is the mass-flow through the slot die. There are multiple methods to pre-meter the slurry, but ultimately, a mechanical pumping system that adjusts a continuous mass flow into the slot die represents the most state-of-the-art method available.[4]

2.2 Slurry and its constituents

While precise pumping techniques might provide the right quantity of slurry for coating from the coating tank, the process to deagglomerate the input materials and homogenise the particle distribution in the dispersion is essential within the mixing process. The standard mixing technique applies a batch method, where the mixing process is divided into dry powder mixing and wet slurry mixing [15]. First, the active material and conductive agents are mixed to deagglomerate the powders. In the second step, a binder is dissolved in a solvent-based (non-aqueous) or waterbased (aqueous) solvent, as the coating must be presented in fluid form. Based on the cathode or anode material being coated, the binder selection is based. For both cathodes and anodes, polyvinylidene fluoride (PVDF) can be used as polymeric binder. The binder enhances the adhesion properties within the coating, as well as at the coating-foil interface. Furthermore, the binder enables a specific elasticity of the electrode coating, which absorbs the mechanical tensions during the intercalation process. The solvent predominantly used for the cathode, in combination with PVDF, is the N-Methyl-2-pyrrolidon (NMP). The usage of the highly toxic NMP results in high cost and safety concerns, but it is still the means of choice. Graphite, which is used as anode active material, naturally possesses a high intrinsic electric conductivity. Nevertheless, a small amount of conductive agent is added as well. While the discussion for the type

of material is critical, [10] the various mixing sequences also has a significant influence on the mixing process quality which includes optimal mass ratio and particle size. The cell capacity and cell cyclability also is influenced with the chronology of adding components (mixing sequences) and mixing methods. Likewise, a pre-mixing and pre-dispersion of particular materials can avoid the formation of agglomerates and enhance cell capacity.[19] Stirring for insufficient duration or application of shear force outside the advised limits can lead to agglomerates and inhomogeneous particle distributions.

2.3 Problem Statement and Objective

Taking a deeper interest in the mixing phenomena, an observation states that some coating processes show non uniformity in terms of composition of particles. A non-uniform composition within the slurry supplied is the core reason behind the abnormality in the coating composition. This non-uniformity within the slurry can be attributed to a specific batch which has been supplied from the transfer tank. Identifying the specific batch that has deviated from homogeneity due to improper mixing might help in fixing further batches. Thus, a proper spatial and time discretization for the transfer tank is required to understand why some batches show erratic properties which are detrimental towards the battery quality.
The setup includes the transfer tank which holds the homogeneous slurry. The slurry it receives has already been homogenized by the slurry mixer. This transfer tank as described by 2.1 contains a stirrer installed within its fuselage to maintain the slurry consistency and prevent the particles within the slurry to settle down. The transfer tank receives the slurry in batches from the mixer. Every batch is supplied to the supply tank once the previous batch reaches a threshold minimum height in the transfer tank. The supply tank maintains uninterrupted supply of slurry to the coating nozzle 2.2

Replicating the above scenario we consider a 800 l transfer tank receiving a batch of 500 l slurry at a give time. Once the batch gets transferred in the coating nozzle through the supply tank, the decreasing height of slurry within the transfer tank is observed. Once the height reaches a threshold bottom, the new batch of slurry is added in the transfer tank. The transfer tank is considered to be a temperature controlled enclosure which thermodynamically can be considered isothermal. The temperature is maintained by the continuous interaction with a liquid bath with a large specific heat.

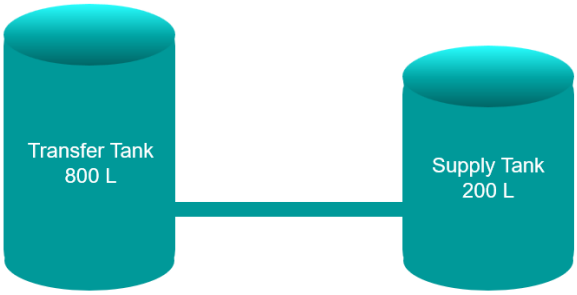

Figure 2.1: Step 1: Supply from Transfer Tank to Coater Tank

The current study focuses on the multiphase aspect of mixing within the tranfer tank and identifying the correct models governing the mixing process. For a three dimensional direct numerical solution, Star CCM + by Siemens has been used. The software provides flexibility in all aspects of fluid modelling hence is suited to simulate complex scenarios. The whole study comprises of three tasks which increase in complexity. The tasks have been performed in order to receive a basic understanding of mixing models, with a goal to increase the complexities of material without changing the physics.

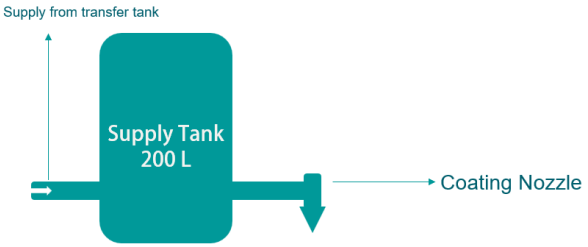

Figure 2.2: Step 2: Transfer from Supply Tank to Coating Nozzle

The tasks with time can be enumerated as following:

1. A simple geometry has been built to understand the fluid flow within a tank for simple water.
2. Varying the rotation speed of the stirrer for validating physics by comparing mixing times and volume uniformity.
3. Varying the mesh resolution of the fluid to verify the optimal mesh size.

Chapter 3

Modelling in Star CCM +

3.1 Basics of Fluid Modelling

Computation Fluid Dynamics (CFD) is a tool used extensively to predict the fluid behaviour across different geometries and understand fluid dynamics. The study of fluid dynamics involves the analysis of various properties exhibited by different fluids under different conditions. In order to accurately simulate fluid behavior, it is crucial to comprehend the nature of the fluid and its flow. While there are numerous variables involved in solving fluid equations, they can be categorized into the following sections from a theoretical standpoint:

- Initial/Boundary Conditions: These conditions define the starting state and constraints imposed on the fluid system, serving as the foundation for any simulation.
- Meshing and Discretization: The process of meshing involves dividing the fluid domain into small discrete elements, facilitating the numerical solution of fluid equations. Proper discretization techniques are crucial for accurate simulations.
- Material Properties: Fluids possess distinct material properties, such as viscosity, density, and thermal conductivity, which significantly influence their behavior. Understanding and incorporating these properties are essential for realistic simulations.
- Solver Functions: Solver functions are mathematical algorithms employed to numerically solve the fluid equations, enabling the prediction of fluid behavior over time.
- Physics (Multiphase Modeling): The study of multiphase flow involves investigating the interactions and behavior of different phases within a fluid system. This encompasses phenomena like phase transitions, interface dynamics, and complex interactions between phases.

3.2 Brief Introduction to Star-CCM+

Among the available commercial solvers, StarCCM + provides great parallelization capabilities with flexibility in terms of choosing solvers and setting up simulations. [18] The software has a great interface which spreads out based on the use case just like a tree with every branch allowing the user to detail the specificity. A typical workflow of Star CCM+ is shown in the image below.

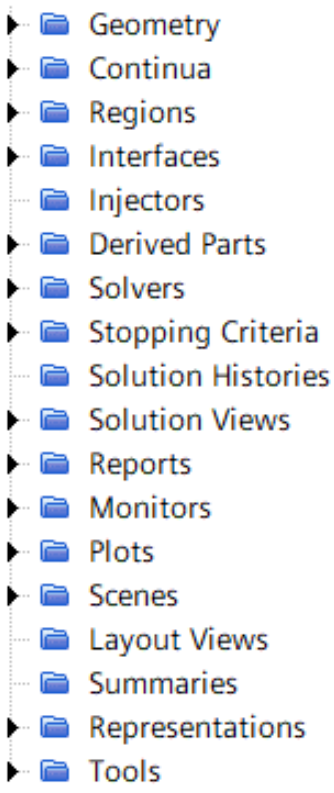

Figure 3.1: Star workflow

The **Geometry** introduces the part and also controls the meshing for the geometry. The **Continua** lets the user define the solvers and material. The **Regions** links the continua with different meshed components and introduces the boundary conditions. The **Interface** defines the interconnections between different regions. The **Derived Parts** allows user to create sections within the mesh, which might be useful for visualizing the results within the solution. **Solvers** helps in governing the time step with varying the courant number along with time-related parameters for solver. **Stopping Criteria** governs the internal iterations, simulation run time and maximum iterations. **Reports, Monitors, Plots and Scenes** are important for Post processing. Plots activates the Residual chart which includes the momentum and energy conservation residuals as default.**Tools** are necessary for introducing field functions which calculate different output parameters. Tools contain multiple features which are intertwined within the simulation and allows user with flexibility for adapting the simulation as per users requirements.

3.3 Overview of the Geometry

A basic supply tank for a coater consists of multiple entry and exit surfaces. A mixing process involves a stirrer which has been included in the tank. The following figure explains the geometry.

3.3.1 Tank

The tank contains the velocity inlet, pressure outlet and mass flow outlet for the fluid movement. Considering the problem statement, a 800 l tank is not feasible for simulation, it has been scaled to the dimensions mentioned in table 3.4. The tank houses the rotating cylinder and the stirrer. The default material for the tank volume is water, the tank shell is selected to be aluminium.

3.3.2 Rotating Cylinder and Stirrer

The rotating cylinder has been created to imitate the fluid rotation across the stirrer. The stirrer has been modelled to rotate the fluid within the tank volume. The rotating cylinder section within the tank has been separated to account for the overset mesh required during stirrer rotation. The cylinder is thus rotated with rpm required keeping the outer tank volume to remain stationary. The tank volume and rotating cylinder are connected using the Interface 1, which are connected using the imprint function within Star-CCM+ to create a single part surface. The interface

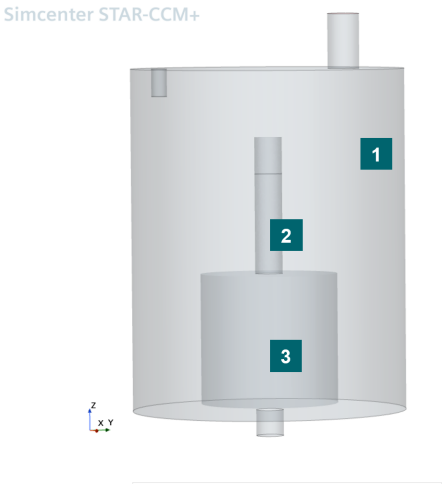

Figure 3.2: Assembled Geometry

Numbering	Geometry Name
1	Tank
2	Rotating Cylinder
3	Stirrer

Figure 3.3: Geometry Numbering

Features	Dimension
Tank Height	0.028 m
Tank Radius	0.001 m
Stirrer Radius	0.00025
Rotating Cylinder Radius	0.0005
Rotating Cylinder Height	Table cell 4

Figure 3.4: Dimensions of the Geometry

automatically refines the overset meshes thus calculating the correct momentum transfers between the two section 3.5. A similar interface has been defined for the stirrer and rotating cylinder with 'in-place' interface. The 'in-place interface' creates a single topology for the intersecting surfaces between the two bodies which have been defined. It adjusts after every iteration . The shaded red, green, and blue areas in the figure 3.7 represents different mesh regions, such as porous/non-porous or fluid/solid combinations. The dotted black line in each case would represent the in-place interface that would be created between the coincident boundaries for each region.

3.4 Meshing and Discretization

3.4.1 Theory

Meshing

Meshing process encompasses the following features which the user must define based on use-case:
Mesh Resolution: While the coarser mesh reduces the computational effort, higher resolution provides accuracy at the cost of higher computational resources. The balance is studied using grid independence test which determines the change in order of results with increase in mesh resolution.
Mesh Density: The number of cells in the mesh affects the spatial resolution of the simulation. Higher mesh density captures small-scale flow phenomena accurately but requires more computational resources and time.
Mesh Type: Different types of meshes, such as structured, unstructured, or adaptive, have their advantages and limitations. Structured meshes offer regular cell arrangements and efficient numerical schemes, but they are often restricted to simpler geometries. Unstructured meshes allow for complex geometries but may require more computational resources. Adaptive meshes dynamically refine or coarsen regions based on flow conditions, improving accuracy while minimizing computational costs.
Boundary Layer Resolution: The mesh near solid boundaries needs to be refined to capture the boundary layer, where flow behavior is significantly influenced by wall effects. Proper resolution of the boundary layer is crucial for accurate predictions of flow separation, shear stress, and

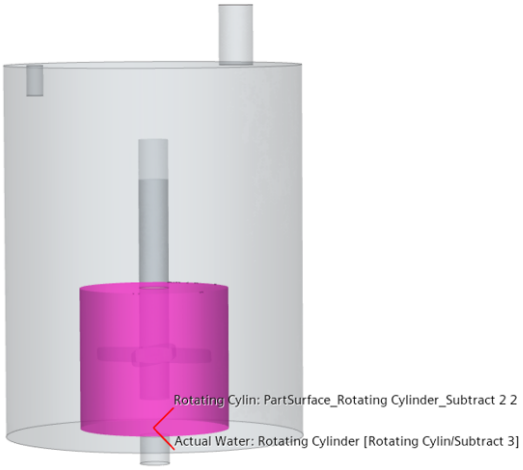

Figure 3.5: Interface 1

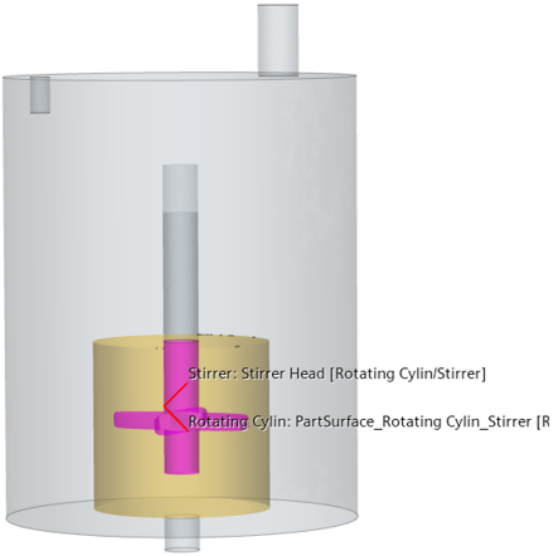

Figure 3.6: Interface 2

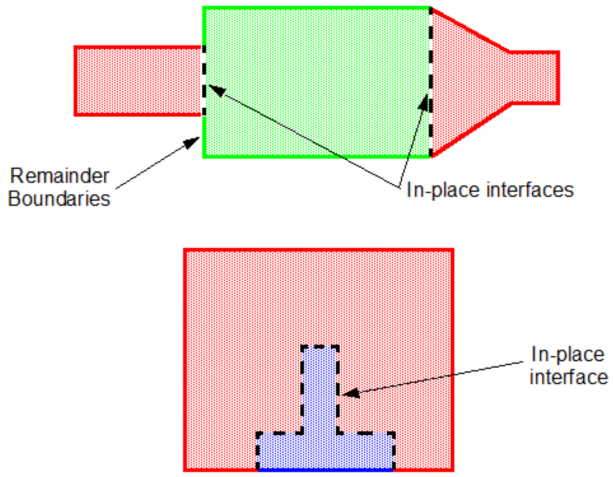

Figure 3.7: In-Place Interface

heat transfer.

Discretization

Discretization can be temporal or spatial in nature based on time stepping and position stepping respectively. Temporal discretization can be implicit or explicit. Implicit schemes takes values from future time step along with the current time step to calculate the result whereas explicit schemes use values from current time step only.[12]. Numerical schemes are chosen based on the partial differential equations to be discretized. The choice of scheme affects the stability, accuracy, and computational efficiency of the simulation. Implicit schemes are generally more stable but computationally costlier than explicit schemes.

Stability and CFL Condition Stability is a crucial consideration in numerical simulations. The Courant-Friedrichs-Lewy (CFL) condition imposes restrictions on the time step size based on the grid spacing and velocity field to ensure stability. Coarser grids or higher velocities require

smaller time steps to satisfy stability conditions. The CFL condition refers to the courant number ($C = u\frac{\Delta t}{\Delta x}$) being always lesser than 1, such that the physical time step size to spatial step size ratio ($\frac{\Delta t}{\Delta x}$) is always covered by the numerical time step $\frac{dt}{dx}$.
Convergence Discretization affects the convergence behavior of the simulation. Properly designed and implemented discretization schemes should converge to the correct solution as the grid is refined.

Adaptive Mesh Refinement

The numerical technique of Adaptive Mesh Refinement (AMR) is a great tool used in simulations to dynamically adjust the computational grid to better capture complex phenomena. This feature present in the Star-CCM+ selectively refines or coarsens the mesh based on predefined criteria or error indicators. By refining the mesh in regions of interest and coarsening it in less critical areas, AMR improves accuracy and reduces computational cost. The adaptive process is typically iterated until a desired level of accuracy or convergence is achieved, allowing simulations to efficiently resolve features such as shocks, boundary layers, and other regions with high gradients. The current work involves usage of Free-Surface Adaptive Mesh Refinement (FS-AMR) which is a technique used in Star-CCM+ to dynamically adapt the computational mesh to accurately capture the behavior of liquid-gas and liquid-liquid interactions with a free surface. FS-AMR is a valuable technique for accurately simulating and analyzing liquid-gas interactions with a free surface. The free surface provides accurate representation which is crucial for capturing phenomena such as droplet formation, coalescence, breakup, and complex flow patterns. The figure below represents the free surface mesh which clearly shows the refined parts which are created automatically by the software to accurately calculate parameters at the interfaces.

3.5 Material Properties

Material properties play a crucial role in computational fluid dynamics (CFD) simulations as they directly influence the behavior and characteristics of the fluid flow. These properties can significantly impact the accuracy and reliability of the simulation results. Here are a few key ways in which material properties affect CFD simulations:
Density and Viscosity: The density and viscosity of a fluid determine its behavior in terms of flow velocity, turbulence, and resistance to deformation. Higher density fluids require more force to accelerate and can result in different flow patterns compared to lower density fluids. Viscosity affects the internal friction of the fluid and influences flow resistance and boundary layer development. Accurate representation of these properties is crucial for capturing flow characteristics and predicting pressure drops, shear stresses, and turbulence.
Thermal Conductivity and Specific Heat: Fluids with different thermal properties exhibit varying heat transfer characteristics. Thermal conductivity determines how efficiently heat is conducted through the fluid, while specific heat determines the amount of energy required to raise the fluid's temperature. These properties affect temperature distribution, convective heat transfer, and the development of thermal boundary layers.
Compressibility: Compressible fluids, such as gases, exhibit significant changes in density with variations in pressure and temperature. Compressibility effects, including shocks, expansion waves, and rarefaction waves, must be properly accounted for in simulations involving high-speed flows or significant pressure variations. Accurate modeling of compressibility is crucial to capture the correct flow behavior and pressure distribution.

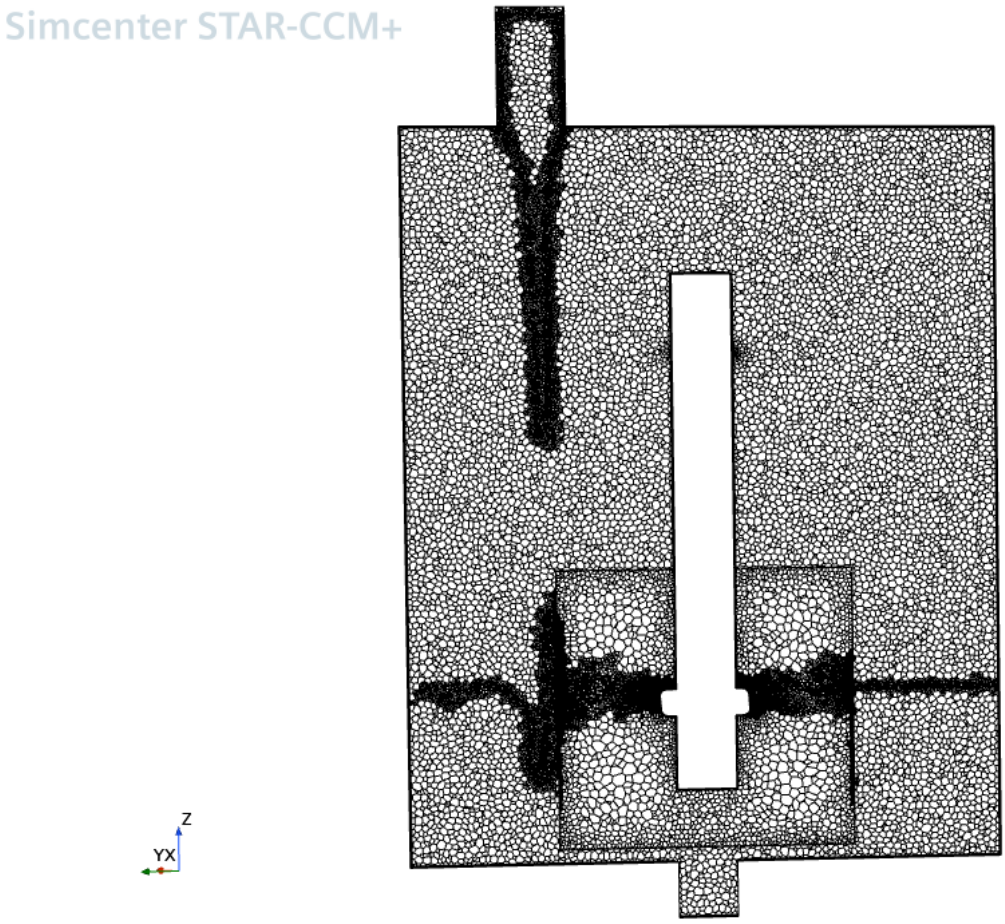

Figure 3.8: Cross-Section Mesh

Surface Tension: Surface tension is particularly important in simulations involving free surfaces or multiphase flows. It affects the shape, stability, and breakup of interfaces between different phases, such as liquid-liquid or liquid-gas interactions. Properly representing surface tension is crucial for accurately predicting droplet dynamics, capillary effects, and interfacial behavior.
Chemical Properties: In simulations involving reactive flows or species transport, chemical properties such as reaction rates, diffusion coefficients, and solubility can significantly impact the simulation results. These properties govern chemical reactions, species transport, and mixing processes, making them critical for simulations involving combustion, chemical reactors, and pollutant dispersion.
Accurate and reliable representation of material properties is essential for obtaining meaningful and realistic results from CFD simulations. The selection and input of appropriate material properties based on experimental data or theoretical models are crucial steps in ensuring the fidelity of the simulation and its relevance to real-world scenarios.

3.6 Solver Functions

The fluid flow can be represented using the navier-stokes equations. These equations contain the necessary variables which are either given in the initial or boundary conditions or need to be solved. The equations broadly contain three different conservation equations:

3.6.1 Conservation of Mass

In absence of source term or sink term, we assume that the mass inflow and outflow of a fluid cell is constant. It can be denoted as:

$$\frac{\partial}{\partial t}(\rho)+\frac{\partial}{\partial x}(\rho\cdot u)+\frac{\partial}{\partial y}(\rho\cdot v)+\frac{\partial}{\partial z}(\rho\cdot w)=0 \tag{3.1}$$

3.6.2 Conservation of Momentum

Momentum conservation is generally observed in cases where sudden external forces are absent within the system. They can be expressed by:

$$\frac{\partial}{\partial t}(\rho\cdot u)+\frac{\partial}{\partial x}\left(\rho\cdot u^2+\rho-\tau_{xx}\right)+\frac{\partial}{\partial y}\left(\rho\cdot u\cdot v-\tau_{yx}\right)+\frac{\partial}{\partial z}\left(\rho\cdot u\cdot w-\tau_{zx}\right)-\rho\cdot g_x=0 \tag{3.2}$$

$$\frac{\partial}{\partial t}(\rho\cdot v)+\frac{\partial}{\partial x}\left(\rho\cdot v\cdot u-\tau_{xy}\right)+\frac{\partial}{\partial y}\left(\rho\cdot v^2+\rho-\tau_{yy}\right)+\frac{\partial}{\partial z}\left(\rho\cdot v\cdot w-\tau_{zy}\right)-\rho\cdot g_y=0 \tag{3.3}$$

$$\frac{\partial}{\partial t}(\rho\cdot w)+\frac{\partial}{\partial x}\left(\rho\cdot w\cdot u+\tau_{xz}\right)+\frac{\partial}{\partial y}\left(\rho\cdot w\cdot v-\tau_{yz}\right)+\frac{\partial}{\partial z}\left(\rho\cdot w^2+\rho-\tau_{zz}\right)-\rho\cdot g_z=0 \tag{3.4}$$

3.6.3 Conservation of Energy

The energy conservation is important when there are added source terms within the equationsin the form of Enthalpy or Mass inlet. The same can be written in the form:

$$\frac{\partial}{\partial t}\left[\rho\cdot\left(e+\frac{1}{2}\cdot\vec{u}^2\right)\right]+\frac{\partial}{\partial x}\left[\rho\cdot u\cdot\left(h+\frac{1}{2}\vec{u}^2\right)-\left(u\cdot\tau_{xx}+v\cdot\tau_{xy}+w\cdot\tau_{xz}\right)-\lambda\frac{\partial T}{\partial x}\right] \tag{3.5}$$

$$+\frac{\partial}{\partial z}\left[\rho\cdot w\cdot\left(h+\frac{1}{2}\vec{u}^2\right)-\left(u\cdot\tau_{zx}+v\cdot\tau_{zy}+w\cdot\tau_{zz}\right)-\lambda\frac{\partial T}{\partial z}\right]-\rho\cdot\left(u\cdot g_x+v\cdot g_y+w\cdot g_z\right)=0$$

The user can refer to the CFD Book [12] for getting a deeper understanding of the equations.

3.7 Multiphase Flow Modelling

Multiphase flow refers to the simultaneous movement of multiple phases, such as gas, liquid, and solid particles, within a system. Modeling multiphase flow is a complex task that involves understanding the interactions between different phases and accurately predicting their behavior. Here's a brief explanation of how multiphase flow can be modeled:

3.7.1 Continuum Approach

The continuum approach treats the multiphase flow as a continuous medium with averaged properties. It assumes that each phase occupies a portion of the system, and the flow behavior can be described by macroscopic equations, such as the navier-stokes equations. In this approach, conservation laws for mass, momentum, and energy are applied to each phase, considering interfacial interactions and phase transitions. A simple hagen–poiseuille flow utilizes the average values of velocities to evaluate the pressure difference across a pipe which is a classic example for this approach.

3.7.2 Two-Fluid Model

The two-fluid model is a widely used approach in multiphase flow modeling. It assumes that the mixture is composed of two interpenetrating continua: the continuous phase and the dispersed phase. The model considers the separate conservation equations for each phase, accounting for interfacial forces, phase interactions, and phase distribution. Fluidized beds use the two phase flows for evaluating the air entrained by the fluid.

3.7.3 Eulerian-Eulerian Approach

The Eulerian-Eulerian approach treats each phase as a separate continuous medium with its own set of governing equations. It tracks the phase volume fractions and velocities of each phase throughout the system. The interaction between phases is modeled through interfacial terms, such as drag forces and interphase mass and heat transfer. Fluids mixing out of gravity in open channel flows can be modelled using this approach.

3.7.4 Discrete Element Method (DEM)

In cases where solid particles are involved in the multiphase flow, the discrete phase model is employed. This model treats the particles as Lagrangian entities and tracks their individual trajectories and interactions with the fluid phases. It accounts for particle-particle and particle-fluid interactions, considering forces like drag, gravity, and interparticle collisions. The battery production process uses DEM for evaluating the coupling forces between solid-solid and solid-liquid.

3.7.5 Reynolds-Averaged Navier-Stokes(RANS)

The Navier-Stokes equations, which govern the motion of fluid, are averaged over time in the RANS approach, resulting in a time-averaged representation. The purpose of this averaging is to separate the mean flow variables from the fluctuating turbulent quantities.The equations in x, y and z direction are solved numerically to obtain the mean velocity and pressure fields in the flow domain.To close the RANS equations, a turbulence model is employed. Turbulence models approximate the effects of turbulent fluctuations on the mean flow by introducing additional transport equations for turbulent quantities, such as turbulence kinetic energy and its dissipation rate. There are different types of turbulence models available for RANS simulations, like:

k-epsilon Model

The k-epsilon model is a two-equation turbulence model that solves transport equations for turbulence kinetic energy (k) and its dissipation rate (epsilon). It is widely used in many engineering applications due to its simplicity and robustness.

k-omega Model

The k-omega model is another two-equation turbulence model that solves transport equations for turbulence kinetic energy (k) and the specific dissipation rate (omega). It is known for its ability to handle adverse pressure gradient flows and boundary layer separation.

3.7.6 Volume-of-Fluid (VOF) Method

The VOF method [9] is commonly used for modeling multiphase flows with distinct interfaces. It tracks the volume fraction of each phase within a computational cell and uses interface capturing techniques to accurately represent the interface shape and motion. The VOF method is particularly useful for free surface flows and phase separation.

3.8 Fluid Flow Modelling

The fluid flow motion has been visualized to flow in the tank which contains some initial liquid and air. The complete fluid flow is multiphase in nature. The different interactions can be ennumerated as:

1. Liquid Gas Interaction
2. Liquid Liquid Interaction
3. Liquid Solid Interaction

3.8.1 Liquid Gas Interaction

The Liquid Gas interaction is modelled using Volume of Fluid (VOF) method with interface tracking using High Resolution Interface Capturing(HRIC). The VOF method equations are as follows:
The volume fraction equation:

$$\frac{\partial \alpha}{\partial t} + \nabla \cdot (\alpha \mathbf{u}) = 0 \tag{3.6}$$

The momentum equation:

$$\rho \left(\frac{\partial \mathbf{u}}{\partial t} + \mathbf{u} \cdot \nabla \mathbf{u} \right) = -\nabla p + \nabla \cdot (\mu (\nabla \mathbf{u} + \nabla \mathbf{u}^T)) + \rho \mathbf{g} + \nabla \cdot \left(\alpha (1-\alpha) \frac{\sigma}{\rho} \kappa \nabla \alpha \right) \tag{3.7}$$

Here, α represents the volume fraction of the fluid, $\mathbf{u}$ is the velocity vector, t is time, ρ is the density, p is the pressure, μ is the dynamic viscosity, $\mathbf{g}$ is the gravitational acceleration vector, σ is the surface tension coefficient, and κ is the curvature.

3.8.2 Liquid Liquid Interaction

The Liquid liquid interaction is considered homogenous in nature and homogeneity can be measured using the uniformity of volume fraction. The Passive Scalar tool available in the Star-CCM+ (explained in the next section) has been used to visualize the Fluid Fluid interaction.

Passive Scalar Mixing

Passive scalars are user-defined variables of arbitrary value, assigned to fluid phases or individual particles. They are passive because they do not affect the physical properties of the simulation. An intuitive way to think of passive scalars is as tracer dye in a fluid, but with numerical values instead of colors, and with no appreciable mass or volume. The geometry below has been created

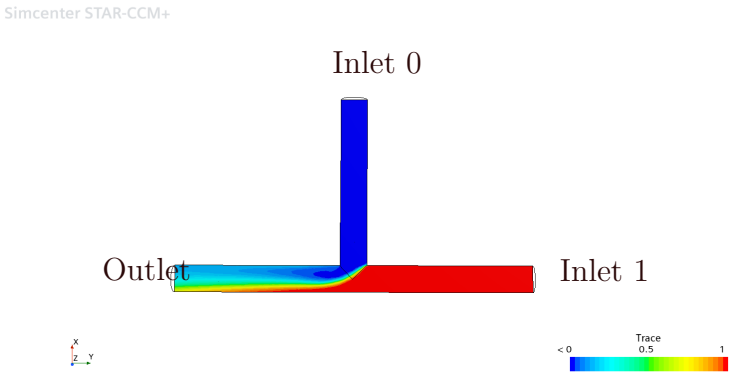

Figure 3.9: T Joint Liquid-liquid interaction

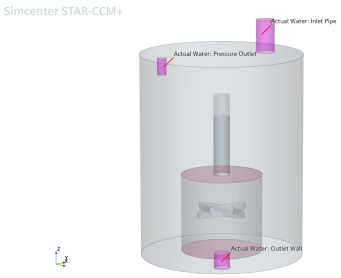

Figure 3.10: Prism Layer Exceptions

to provide an insight how passive scalar works.

T Section Geometry

The Passive Scalar can be depicted within a T geometry which has been simulated to understand its usage.

- A T Joint has been modelled in order for the fluid to mix across two inputs with the different colours depicting the mixture occurring when the fluids are mixed.
- The top side of the T Joint and right side have been modelled as the inlets for Fluid.
- The vertical inlet section contains fluid with passive scalar value as 0.
- The second horizontal inlet 1 contains the passive scalar value of 1.
- The mixing produces values ranging from 0 to 1. The mixed scalar defines the volume uniformity which is visible at a steady state which occurs at a much further time step.

3.8.3 Liquid Solid Interaction

The liquid solid interaction has been defined with 3-10 prism layers at different boundaries based on geometry with boundary layer formation within the cross section. The prism layers have been exempted in the areas of inlet, mass flow outlet and pressure outlet as shown in the 3.10. The y+ parameters have been set with 10% growth rate across the boundary.

Chapter 4

Tasks

4.1 Task I: Running the first mixing simulation

As an initial step to understand the mixing, the tank with dimensions mentioned in Table 3.4 has been modelled in Siemens NX.

4.1.1 Initialization

Boundary and Initial Condition

- The tank inlet is made to receive an inflow of 0.45 Liters/min fluid.
- The pressure outlet is kept at 1 atm. This allows any pressure buildup in air, during water inflow, to move out.
- The water is filled upto a height of 0.025 m such that the blades are submerged within the fluid.
- The rotating cylinder is stationary initially and gradually increases to a threshold rpm which has been case-wise varied.
- Fixed rpm for Stirrer at 60 rpm.

Solver Function

The space time discretization has been modelled for implicit unsteady conditions with a restriction in the CFL number till 0.8. The lower end has been fixed to 0.2. With multiple iterations run, the residual of passive scalar was carefully observed so as to decrease with time without any oscillations. The following models were implemented as a part of the conitnua for the fluid:

- Free Surface Adaptive Mesh
- Implicit Unsteady
- K- ε Turbulence
- Lagrangian Multiphase
- Reynolds-Averaged Navier Stokes Equation
- Volume of Fluid Method

All the models have been in detail explained in the previous chapter.

Meshing and Discretization

The inner section has been extracted from the 'Extract Geometry' feature within the Star CCM+ model. With a base size of 0.0001 m, the complete fluid region has been meshed with the following features:

- General Cylindrical Mesher
- Prism Layer Mesher
- Polyhedral Mesher
- Advanced Surface Repair

The meshes for Solid part for the Stirrer:

- Polyhedral Mesher
- General Surface Remesher

The rotating cylinder and the tank volume have been imprinted using the imprint feature in Star CCM+. This results on creating a single surface and thus a single tessalated surface is created which is identical for both.

Materials Properties

There are two important material classes which is incorporated in the model:

- Fluid : Water has been selected for the current work as the internal volume.
- Solid : Aluminium has been selected as the material for Stirrer.

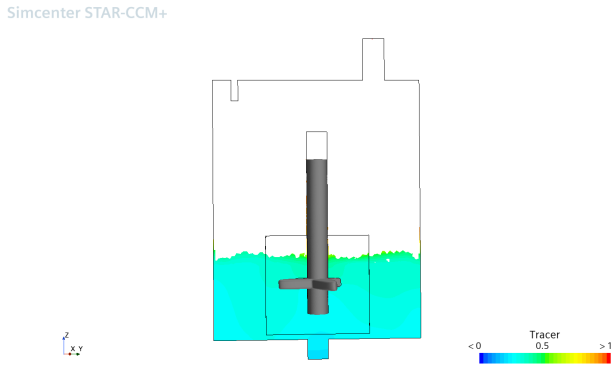

Figure 4.1: Homogenized after Mixing

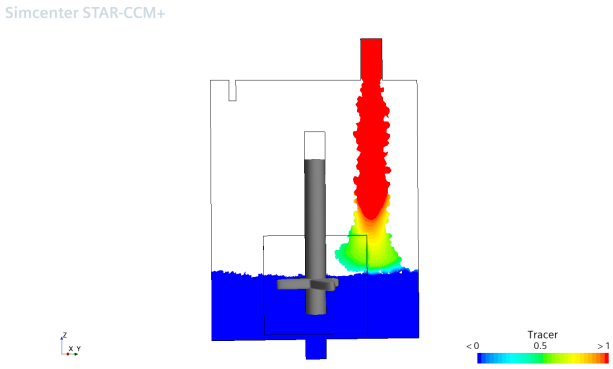

Figure 4.2: Water Inlet

4.1.2 Results

With this task, the model was able to simulate the mixing without any abrupt changes in the **Residuals**. The internal iterations were set to be 5 which explains the spikes after every 5 iterations.

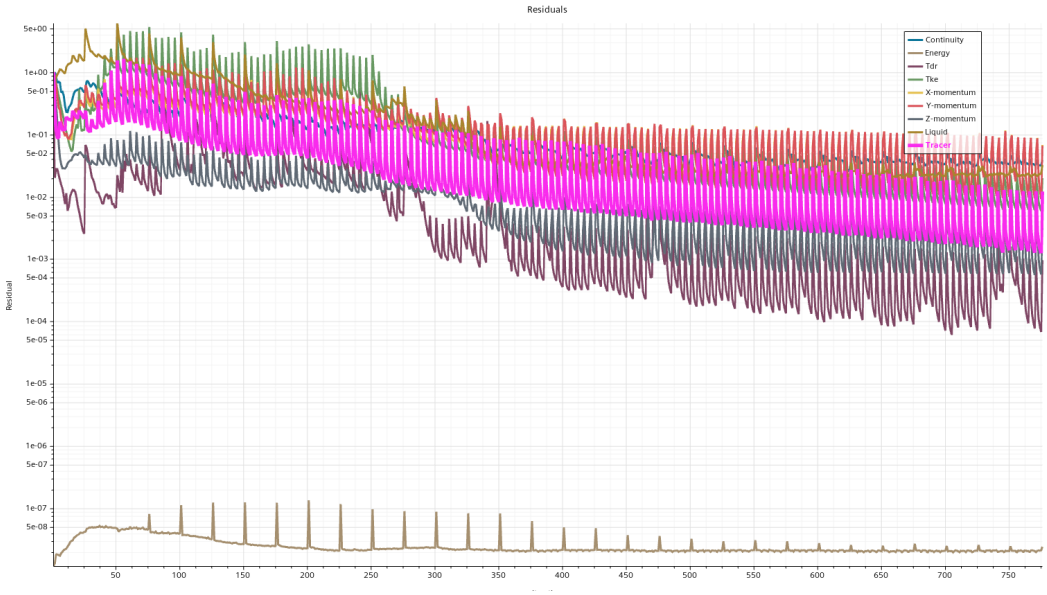

Figure 4.3: Residuals

4.2 Task II: Varying the rotation speeds of the Stirrer

As discussed earlier, mass diffusion is a slow process for achieving 100% mixing, which is the reason for adding stirrer within the tank. A forced convection across the cross-section, increases the Sherwood number which ultimately accounts for an increase in the Turbulent Kinetic Energy(TKE). Higher TKE results in reduction within mixing time[17]. The same principle has been used for this task, where an rpm increase for the stirrer should result in reduction of mixing time. The stirrer rotation speeds have been increased from 60 rpm to 1000 rpm as per table 4.5. The mixing time in the table 4.5 refers to the time taken by the entering fluid (Passive Scalar=1)

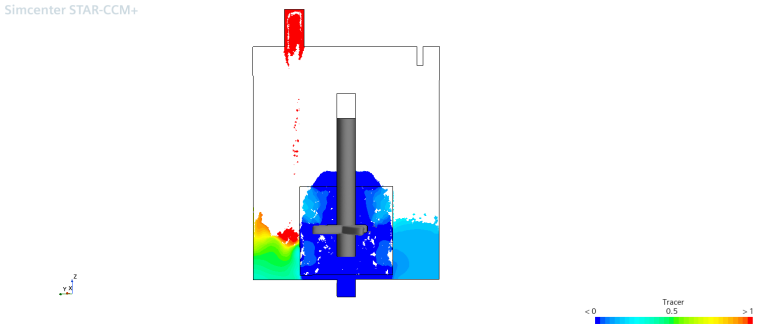

Figure 4.4: Fluid Separation

RPM	Iterations
60	532
100	333
150	218
300	149
500	No Result
1000	No Result

Figure 4.5: Iteration vs RPM

to completely mix with the initial liquid(passive scalar=0) and become a homogeneous mixture(passive scalar=0.5).
A decrease in the mixing time is observed in regards to the iteration needed up till 300 rpm. Owing to the geometry of the mixing tank, the speeds of 500 rpm and 1000 rpm lead to separation of the fluid section in two different parts. The scale of vortices generated due to the excessive TKE results in a pressure difference across the upper liquid section and the lower liquid section allowing the air to penetrate and divide the liquid section. The figure 4.4 shows the issues with running the stirrer at 500 rpm and 1000 rpm.

4.3 Task III: Grid Independence Test

The grid independence test has been performed to asses the best mesh size for the polyhedral mesh. Considering the base size of 1 x 10^{-4} to be refined, the mesh is coarsened to 5 x 10^{-3} and subsequently to 1 x 10^{-3} for a stirrer rotation at 100 rpm. Although identifying a convergence criteria is needed to asses whether coarsening the mesh is beneficial, it becomes difficult to choose a factor as multiple parameters are intertwined. Following are the observations:

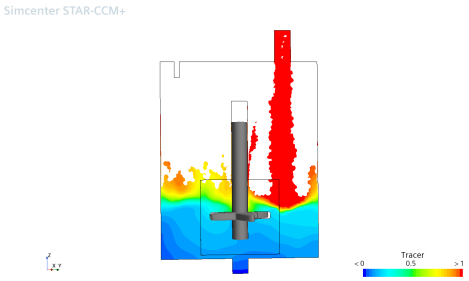

Figure 4.6: Mixing in a mesh size of 1x10^{-3}

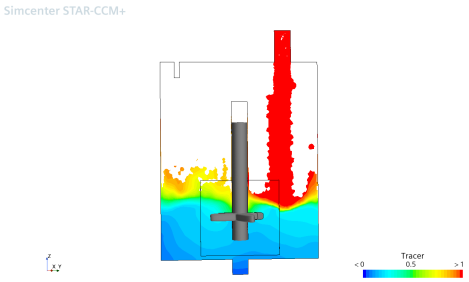

Figure 4.7: Mixing in a mesh size of 5x10^{-3}

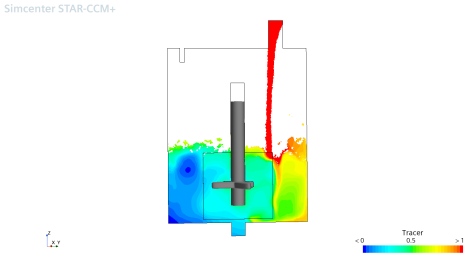

Figure 4.8: Mixing in a mesh size of 1x10^{-4}

Mesh Size	Iterations
1x10^{-4}	333
5x10^{-3}	324
1x10^{-3}	312

Figure 4.9: Mesh Size vs Iteration

- At the mixing front, we observe the iterations needed to reach volume uniformity are almost similar despite reduction in mesh size with the coarsest mesh reaching volume uniformity slightly faster than refined mesh.
- Though the mixing was faster as shown in the table 4.9 the interface between the rotating cylinder and the tank volume looks absurd.
- The water-air interaction surfaces are not smooth and hence is not able to calculate the correct entrainment values.
- Considering VOF method being highly dependent on the cell size, the accuracy with respect to interface formation during inlet and mixing is highly affected by the cell size. While the initial two base sizes were faster in achieving volume uniformity, there were abrupt physics which were observed with same. The interface at the rotational part is critical for the simulation to replicate the correct physics and hence the base size of 1 x 10^{-4} was the best mesh size. Further refinement lead to extremely high computational power which wasn't possible with the current technical specifications.

Chapter 5

Conclusion

The current model is able to simulate and distinguish two different fluids which are mixing and homogenizing with time. The task wise separation leads us to different conclusions which can be summarized as:

- With the design of tank and stirrer geometry, the model is able to simulate the water inlet, the mixing and volume uniformity at the end. The passive scalar, a tool in the Star CCM+ software, provides a clear depiction of the water inlet, mixing and the homogeneity getting achieved due to the added turbulence from stirring.
- The mixing time within the tank is a great way to test whether the simulation is able to replicate the physics. While there is a decreasing trend in the mixing time with increasing rpm (as a measure of the iterations needed), an increase further from 500 rpm, leads to excessive turbulence resulting in separation within the fluid which results in uneven mixing.
- The final grid independence test checks whether the mixing performance gets affected due to finer mesh. While refining mesh, increases the computational time extensively, reducing the mesh size lead to reduction in mixing time to a minor extent. But the interfaces look abrupt for the first two meshes, which result in unreliable physics for higher rpm, making them unfeasible. This helped in concluding the base size of 1 x 10^{-4} is appropriate for the model.

With the current study targeting the mixing models, it helps understand how homogeneous slurries behave when mixed in batches. The future course can be :

- Adding non-newtonian fluids
- Inserting particles for active material and binders
- Changing stirrer blade geometries and checking the behaviour
- Coupling the simulation with coating and observing coating variations with respect to mixing parameters.

Bibliography

[1] *Battery Production Process*. URL: https://www.pem.rwth-aachen.de/global/show_document.asp?id=aaaaaaaaabdqbtk (visited on 07/07/2023).

[2] Henrike Bockholt et al. "The interaction of consecutive process steps in the manufacturing of lithium-ion battery electrodes with regard to structural and electrochemical properties". In: *Journal of Power Sources* 325 (Sept. 2016), pp. 140–151. DOI: 10.1016/j.jpowsour.2016.05.127. URL: https://doi.org/10.1016/j.jpowsour.2016.05.127.

[3] Y.-H. Chen et al. "Selection of Conductive Additives in Li-Ion Battery Cathodes". In: *Journal of The Electrochemical Society* 154.10 (2007), A978. DOI: 10.1149/1.2767839. URL: https://doi.org/10.1149/1.2767839.

[4] Claus Daniel and Jürgen O. Besenhard, eds. *Handbook of Battery Materials*. Wiley, Aug. 2011. DOI: 10.1002/9783527637188. URL: https://doi.org/10.1002/9783527637188.

[5] Mahmoud A. El-Emam et al. "Theories and Applications of CFD–DEM Coupling Approach for Granular Flow: A Review". In: *Archives of Computational Methods in Engineering* 28.7 (Apr. 2021), pp. 4979–5020. DOI: 10.1007/s11831-021-09568-9. URL: https://doi.org/10.1007/s11831-021-09568-9.

[6] Desiree Grießl et al. "Effect of the Slurry Mixing Process on the Structural Properties of the Anode and the Resulting Fast-Charging Performance of the Lithium-Ion Battery Cell". In: *Journal of The Electrochemical Society* 169.2 (Feb. 2022), p. 020531. DOI: 10.1149/1945-7111/ac4cdb. URL: https://doi.org/10.1149/1945-7111/ac4cdb.

[7] Xuechen He et al. "Constructing a conductive and buffer network on microscale silicon-based anodes for high-performance lithium-ion batteries". In: *Journal of Alloys and Compounds* 949 (July 2023), p. 169846. DOI: 10.1016/j.jallcom.2023.169846. URL: https://doi.org/10.1016/j.jallcom.2023.169846.

[8] Alexander Hoffmann et al. "CFD model of slot die coating for lithium-ion battery electrodes in 2D and 3D with load balanced dynamic mesh refinement enabled with a local-slip boundary condition in OpenFOAM". en. In: (2022). DOI: 10.5445/IR/1000151271. URL: https://publikationen.bibliothek.kit.edu/1000151271.

[9] Nikolaos D. Katopodes. "Chapter 12 - Volume of Fluid Method". In: *Free-Surface Flow*. Ed. by Nikolaos D. Katopodes. Butterworth-Heinemann, 2019, pp. 766–802. ISBN: 978-0-12-815485-4. DOI: https://doi.org/10.1016/B978-0-12-815485-4.00018-8. URL: https://www.sciencedirect.com/science/article/pii/B9780128154854000188.

[10] Kwang Man Kim et al. "Effect of mixing sequences on the electrode characteristics of lithium-ion rechargeable batteries". In: *Journal of Power Sources* 83 (1999), pp. 108–113.

[11] Reiner Korthauer, ed. *Handbuch Lithium-Ionen-Batterien*. Springer Berlin Heidelberg, 2013. DOI: 10.1007/978-3-642-30653-2. URL: https://doi.org/10.1007/978-3-642-30653-2.

[12] Reiner Korthauer, ed. *Lithium-Ion Batteries: Basics and Applications*. Springer Berlin Heidelberg, 2018. DOI: 10.1007/978-3-662-53071-9. URL: https://doi.org/10.1007/978-3-662-53071-9.

[13] Amit Mishra et al. "Electrode materials for lithium-ion batteries". In: *Materials Science for Energy Technologies* 1.2 (Dec. 2018), pp. 182–187. DOI: 10.1016/j.mset.2018.08.001. URL: https://doi.org/10.1016/j.mset.2018.08.001.

[14] M. Nikpour, B. A. Mazzeo, and D. R. Wheeler. "A Model for Investigating Sources of Li-Ion Battery Electrode Heterogeneity: Part II. Active Material Size, Shape, Orientation, and Stiffness". In: *Journal of The Electrochemical Society* 168.12 (Dec. 2021), p. 120518. DOI: 10.1149/1945-7111/ac3c1f. URL: https://doi.org/10.1149/1945-7111/ac3c1f.

[15] Marcel Schmitt. "Slot die coating of lithium-ion battery electrodes". PhD thesis. Karlsruher Institut für Technologie (KIT), 2016. 171 pp. ISBN: 978-3-7315-0477-1. DOI: 10.5445/KSP/1000051733.

[16] Zhihao Shen et al. "A resolved CFD-DEM coupling model for modeling two-phase fluids interaction with irregularly shaped particles". In: *Journal of Computational Physics* 448 (Jan. 2022), p. 110695. DOI: 10.1016/j.jcp.2021.110695. URL: https://doi.org/10.1016/j.jcp.2021.110695.

[17] Katepalli R. Sreenivasan. "Turbulent mixing: A perspective". In: *Proceedings of the National Academy of Sciences* 116.37 (Dec. 2018), pp. 18175–18183. DOI: 10.1073/pnas.1800463115. URL: https://doi.org/10.1073/pnas.1800463115.

[18] *Star CCM+*. URL: https://plm.sw.siemens.com/en-US/simcenter/fluids-thermal-simulation/star-ccm/ (visited on 07/07/2023).

[19] Hai Yen Tran et al. "Influence of electrode preparation on the electrochemical performance of LiNi0.8Co0.15Al0.05O2 composite electrodes for lithium-ion batteries". In: *Journal of Power Sources* 210 (July 2012), pp. 276–285. DOI: 10.1016/j.jpowsour.2012.03.017. URL: https://doi.org/10.1016/j.jpowsour.2012.03.017.

[20] *Winding*. URL: https://www.tobmachine.com/blog/battery-electrode-winding-process_b50#:~:text=Battery%20electrode%20winding%20is%20the,winding%20for%2018650%20production%20line (visited on 07/07/2023).

[21] Beta Writer. *Lithium-Ion Batteries: A Machine-Generated Summary of Current Research*. Cham: Springer International Publishing, 2019. ISBN: 978-3-030-16799-8 978-3-030-16800-1. DOI: 10.1007/978-3-030-16800-1. URL: http://link.springer.com/10.1007/978-3-030-16800-1 (visited on 07/10/2023).